Nuclear Inst. and Methods in Physics Research, A 904 (2018) 9–14

Contents lists available at ScienceDirect

Nuclear Inst. and Methods in Physics Research, A

journal homepage: www.elsevier.com/locate/nima

Strategies for removing multiple scattering effects revisited

Henrich Frielinghaus

Forschungszentrum Jülich GmbH, Jülich Centre of Neutron Science at Heinz Maier-Leibnitz Zentrum, Lichtenbergstr. 1, D-85747 Garching, Germany

ARTICLE INFO

Keywords:
Small angle neutron scattering
Multiple scattering
Microemulsion

ABSTRACT

The multiple scattering problem of small angle neutron scattering (SANS) is revisited using differential equations from which different contributions are derived. The coherent scattering is connected to multiple scattering events and the ideal single scattering cross sections can be related to the apparent scattering cross section. The multiple scattering problem of the incoherent scattering is more demanding because the sample geometry – I assumed a slab – matters. I tried to solve this problem analytically, and used Monte Carlo simulations. From all concepts I derived a strategy for a computer program that is capable to remove multiple scattering effects. As a side aspect, I could also remove resolution effects.

In this article the multiple scattering problem for small angle scattering is revisited. In early times the methods were developed by Schelten and Schmatz [1], and a program for simulating or removing multiple scattering was proposed by Monkenbusch [2]. The proposed formalism is capable to work on anisotropic scattering patterns. The important prerequisite is that the scattering appears at small angles where the Ewald sphere is flat, and the sample thickness does not vary as a function of the scattering angle. These methods basically apply for the coherent scattering portion while the incoherent scattering needs to be considered separately. For neutrons the incoherent scattering emerges from point scatterers, which facilitates the handling. Whatever radiation is used in the experiment, for my purpose, I assume that the incoherent scattering is rather flat in the experimental q-range, which means that the underlying scattering centers are small compared to $q_{\max}^{-1}$, i.e. the reciprocal largest scattering vector $q_{\max}$. Apart from that, the sample thickness usually varies as a function of the scattering angle. For the slab geometry, basically no signal is detectable in the lateral direction. Early studies from Chandrasekhar [3] focused on the multiple scattering problem quite generally, but the proposed mathematical algorithms do not converge very well. So, even for simple incoherent scattering, the math stays quite difficult.

Our approach uses differential equations for describing the multiple scattering problem. I assume that the different scattering events take place at well-separated points inside the sample, i.e. that the neutron leaves the coherence volume before it is scattered a second time. Coherent multiple scattering would lead to more complicated effects that are known as Mie scattering for light and are also discussed for ultra small angle X-ray scattering [4]. Differential equations make the transfer of neutrons between different channels very clear and the incoherent scattering problem can be implemented easily (see Fig. 1). I distinguish within the channels the primary intensity I_0, the coherently scattered intensity i_1 (as a function of the scattering vector), the incoherent scattered intensity in the forward direction j_+ (as a function of scattering angle), and the incoherent scattered intensity in the backward direction j_-. From all the channels there are outgoing probabilities (proportional to the corresponding scattering cross section), and possibly incoming probabilities. I assumed that a once incoherently scattered neutron does not experience considerably large changes by coherent scattering. The primary intensity, and the coherent scattering can be derived analytically. For the incoherent scattering I tried an analytic approach that makes it difficult to implement boundary conditions. Therefore, I applied Monte Carlo computer simulations to describe the overall multiple scattering of a sample. I chose a microemulsion that scatters strongly enough to generate multiple scattering. From the example I learned which properties of the scattering curves are essential. Then, a general strategy for removing multiple scattering is proposed.

1. Analytical approach for the slab geometry

When describing multiple scattering phenomena analytically, the best way is using differential equations for characterizing the transfer of intensity between different channels. I assumed the slab geometry for the sample with a thickness d. All channels are a function of the normal position x and of the scattering angle ϑ, which also connects to the scattering vector $\mathbf{q}$ with the modulus $q = |\mathbf{q}| = 4\pi \sin(\vartheta/2)/\lambda$. The wavelength of the neutron is λ. Probabilities for the transfer between different channels are described by a cross section and the intensity, from which the contribution emerges. I know the following cross sections for coherent scattering Σ_c, for incoherent scattering Σ_i and for absorption Σ_a (and abbreviate $\Sigma_{ia} = \Sigma_i + \Sigma_a$ and $\Sigma_t = \Sigma_{ia} + \Sigma_c$).

E-mail address: h.frielinghaus@fz-juelich.de.

https://doi.org/10.1016/j.nima.2018.07.027
Received 14 May 2018; Received in revised form 13 June 2018; Accepted 9 July 2018
Available online xxxx
0168-9002/

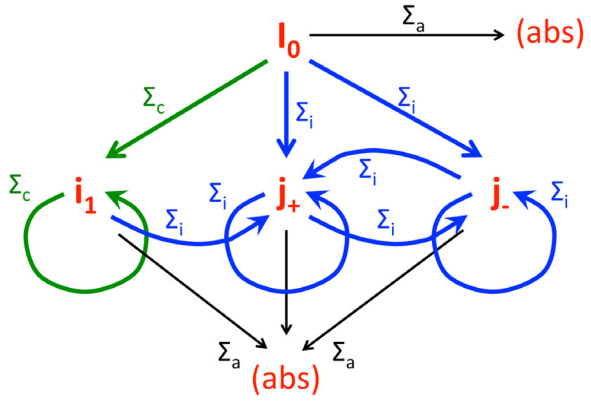

Fig. 1. Explanation for the different channels that neutrons can take from different scattering events. All intensity emerges from the primary intensity I_0, and can end as coherent (i_1) or incoherent scattering in the forward (j_+) or backward (j_-) direction. The scattering probabilities are proportional to the scattering cross sections Σ_x, with x being 'c' for coherent, 'i' for incoherent and 'a' for absorption.

All contributions are summed up, partially from different emerging channels and/or directions, and describe the change of the channel intensity with the position x. In this way, I obtain the following integro differential equations:

$$\partial_x I_0(x) = -\Sigma_t I_0(x) \tag{1}$$

$$\partial_x i_1(x,\mathbf{q}) = \frac{d\Sigma_c}{d\Omega}(\mathbf{q}) I_0(x) + \int \frac{d\Sigma_c}{d\Omega}(\mathbf{q}'-\mathbf{q}) i_1(x,\mathbf{q}') d^2\Omega' - \Sigma_t i_1(x,\mathbf{q}) \tag{2}$$

$$\partial_x j_+(x,\vartheta) = \frac{\Sigma_i}{4\pi}\left(I_0(x) + I_1(x) + \int \frac{j_+ + j_-}{\cos\vartheta} d^2\Omega\right) - \Sigma_{ia}\frac{j_+(x,\vartheta)}{\cos\vartheta} \tag{3}$$

$$-\partial_x j_-(x,\vartheta) = \frac{\Sigma_i}{4\pi}\left(I_0(x) + I_1(x) + \int \frac{j_+ + j_-}{\cos\vartheta} d^2\Omega\right) - \Sigma_{ia}\frac{j_-(x,\vartheta)}{\cos\vartheta} \tag{4}$$

Mathematically, I can distinguish between more channels than experimentally possible (see Fig. 1). The primary intensity I_0 is interpreted as the source beam that only gets weaker inside the sample from scattering processes. The decay of the primary intensity along the normal direction of the slab is described by the differential operator ∂_x, while the probability of the decay is proportional to the total scattering cross section Σ_t and the primary intensity itself. The primary beam takes the full primary intensity $\hat{I}$ at the entrance as one boundary condition. The coherent scattering channels i_1 collect intensity from the primary beam and the other coherent channels due to multiple scattering, and lose intensity for the same reason. The cross-talk (i.e. coherent multiple scattering) between the different scattering channels $i_1(x,\mathbf{q})$ emerges from all coherent scattering channels $i_1(x,\mathbf{q}')$ with the cross talk probability $d\Sigma_c/d\Omega(\mathbf{q}'-\mathbf{q})$. And the range of $\mathbf{q}'$ is connected to the angular range Ω'. On this level, I idealize the 2-dimensional $\mathbf{q}$-plane as flat in contrast to the real Ewald sphere. This means, that I stay in the SANS regime for the coherent single scattering and the multiple scattering. The two incoherent functions $j_\pm$ cover the full angular space in the forward and back direction. So the angle ϑ only covers the half-space (0 to $\pi/2$). The sign of Eq. (4) takes care of the correct orientation of the solid angle. I separated the two half spaces from each other for reasons of the boundary conditions: The back-scattering intensity is zero at the exit of the sample $x = d$, while the forward-scattering takes zero at the entrance $x = 0$ (so does i_1). The effectively longer paths differing from the x-directions are taken into account by the cosine terms (for the incoherent scattering only). One has to keep in mind that, later in the experiment, the coherent scattering and the incoherent scattering in the forward direction superimpose and cannot be distinguished as a bare intensity anymore.

I can define the overall coherent scattering intensity by a similar integration $I_1(x) = \int i_1(x,\mathbf{q}) d^2\Omega = \frac{\lambda^2}{(2\pi)^2}\int i_1(x,\mathbf{q}) d^2\mathbf{q}$. The according differential equation (see Eq. (2)) would read then $\partial_x I_1 = \Sigma_c I_0 - \Sigma_t I_1 + \Sigma_c I_1$. This indicates that the multiple scattering processes do not affect the behavior of the integral coherent intensity. The integral coherent scattering intensity collects intensity from the primary beam and loses intensity to the incoherent channels. Eqs. (3)–(4) treat redistribution effects due to the incoherent scattering only. This means that after a first incoherent scattering process a second coherent scattering process will not show a huge effect. If the main coherent scattering is concentrated at small angles this approximation is quite good and so these possible corrections can be neglected. A wide-angle scattering law introduces atomic and/or molecular structures that are usually observed at large angles and beyond the Ewald sphere. I assume that these contributions are small compared to the incoherent signal, and do especially not show significant multiple scattering. Usually, the content of hydrogenous materials needs to be reasonably high to cause multiple scattering and then the atomistic structures scatter weakly [5].

The different scattering contributions can be solved sequentially. For the primary intensity I obtain $I_0 = \hat{I}\exp(-\Sigma_t x)$. The total coherent scattering is described by $I_1 = \hat{I}(-\exp(-\Sigma_t x)+\exp(-\Sigma_{ia} x))$. It has a maximum at $x = \ln(\Sigma_t/\Sigma_{ia})/\Sigma_c$ and the ideal sample thickness d is chosen accordingly for maximum information of the scattering experiment.

The multiple coherent scattering solution is obtained by using the Fourier transformation. Any function in $\mathbf{q}$-space will be transformed to reciprocal $\mathbf{r}$-space via $\tilde{a}(\mathbf{r}) = \frac{1}{2\pi}\int a(\mathbf{q})\exp(i\mathbf{qr}) d^2\mathbf{q}$. The back-transformation is done by the expression $a(\mathbf{q}) = \frac{1}{2\pi}\int \tilde{a}(\mathbf{r})\exp(-i\mathbf{qr}) d^2\mathbf{r}$. At this point, the formalism describes anisotropic scattering completely right. For isotropic scattering, the Fourier transformation can be carried out in one dimension according to $\tilde{a}(r) = \int_0^\infty a(q) q J_0(qr) dq$ and for the back-transformation according to $a(q) = \int_0^\infty \tilde{a}(r) r J_0(qr) dr$, both known as Hankel transformation of zeroth order. At any point, the reader may go back to anisotropic scattering by dealing with the full vectorial dependence on $\mathbf{r}$. The already well-known [1,2] analytical solution reads then:

$$\tilde{i}_1(d,r) = \hat{I}\frac{2\pi}{\lambda^2}\left(\exp\left(\frac{\lambda^2}{2\pi}\frac{\widetilde{d\Sigma_c}}{d\Omega}(r) d\right) - 1\right)\exp(-\Sigma_t d) \tag{5}$$

This solution also includes the integral intensity solution I_1 according to $\Sigma_c = \frac{\lambda^2}{2\pi}\frac{\widetilde{d\Sigma_c}}{d\Omega}(0)$ and $I_1 = \frac{\lambda^2}{2\pi}\tilde{i}_1(d,0)$. Note, that for small scattering signals the single scattering solution is obtained asymptotically ($\exp(\epsilon) - 1 \approx \epsilon$). The difficulty of this equation is the separation of the incoherent and coherent scattering (say in terms of Σ_c and Σ_i or i_1 and j_+) that will be observed as a sum on the detector. The manuscript will deal with some considerations how to separate these contributions best. The transmission $T = \exp(-\Sigma_t d)$ only measures the total scattering probability Σ_t. The whole Eq. (5) can be solved for the desired macroscopic cross section Σ_c according to:

$$\frac{\widetilde{d\Sigma_c}}{d\Omega}(r) = d^{-1}\cdot\frac{2\pi}{\lambda^2}\cdot\ln\left(\frac{\lambda^2}{2\pi}\frac{\tilde{i}_1(d,r)}{\hat{I}Td} d + 1\right) \tag{6}$$

Again for single scattering processes, the simplification $\ln(\epsilon+1) \approx \epsilon$ leads to the simple absolute calibration formula $d\Sigma_c/d\Omega(q) = i_1(d,q)/(\hat{I}Td)$ that is usually applied to any small angle scattering data. Following this idea, I can define the apparent macroscopic cross section with multiple scattering included.

In the following I discuss how the analytically separated channels add up on the detector and what finite resolution will do to them. The total intensity on the detector is a simple sum of the primary intensity, the coherently and incoherently scattered intensity, according to:

$$i_{tot}(d,\vartheta) = I_0(d)\delta(\vartheta) + i_1(d,q) + j_+(d,\vartheta) \tag{7}$$

The primary intensity without resolution problems has a Dirac-delta shape in the center of the detector. The finite resolution function $R(\langle\vartheta\rangle, \vartheta)$ as a function of the scattering angle ϑ is convoluted with the whole equation. This simply results in the following equation:

$$i_{\mathrm{tot}}(d, \langle\vartheta\rangle) = I_0(d)R(0, \vartheta) + i_1(d, q) \otimes R(\langle q\rangle, q) + j_+(d, \langle\vartheta\rangle) \tag{8}$$

Here, I assumed that the incoherent scattering is not affected by resolution effects (similarly I neglected small angle scattering from already incoherently scattered channels). This equation describes that the primary intensity has the shape of the resolution function at zero scattering angle and the coherent and incoherent scattering intensities superimpose at these small angles, but usually their contribution is so small that the transmission measurement is not affected. If there are doubts the resolution must be increased to separate the primary intensity from the otherwise more flat scattering contributions. The scattered intensity is usually observed next to the shaded primary beam, such that the following separation between coherent and incoherent scattering would hold:

$$i_1(d, q) \otimes R(\langle q\rangle, q) = i_{\mathrm{tot}}(d, \langle\vartheta\rangle) - j_+(d, \langle\vartheta\rangle) \tag{9}$$

In the discussion below I would argue that the incoherent scattering is flat in the small angle range and thus can be determined from the point where the observed scattering levels off. For the deconvolution of both resolution and multiple scattering the following recipe would be obtained:

$$\frac{\widetilde{d\Sigma}_{\mathrm{c}}}{d\Omega}(r) = d^{-1} \cdot \frac{2\pi}{\lambda^2} \cdot \ln\left(\frac{\lambda^2}{2\pi}\frac{\tilde{\imath}_1(d, r)}{\hat{I}Td}\frac{d}{\tilde{R}_{\mathrm{P}}(r)} + 1\right) \tag{10}$$

The resolution function of the approach by Pedersen at al. [6] is primarily based on Gaussian curves. The main argument is that many contributions superimpose and the central limit theorem predicts a Gaussian distribution. The real space resolution function then results in $\tilde{R}_{\mathrm{P}}(r) = \exp(-\sigma^2 r^2/2)$ with the variance of the scattering vector σ with a simple small angle approach $8\ln 2 \cdot \sigma^2 = \left(\langle q\rangle\frac{\Delta\lambda}{\langle\lambda\rangle}\right)^2 + \left(\frac{2\pi}{\langle\lambda\rangle}\frac{3r_1}{2L}\right)^2$ using an optimal resolution of the instrument. Here $\langle q\rangle$ is the q-value where the measurement is done – it varies for each particular q, and so the Hankel transformation has to be done several times. $\Delta\lambda$ is the full width half maximum of the wavelength spread; $\langle\lambda\rangle$ is the actual mean wavelength; r_1 is the radius of the entrance aperture; and L is the collimation length of an optimal SANS setting (with the detector distance being the same). More detailed formulae can be found in Ref. [6].

At the point of Eq. (10) (or Eq. (6)) the absolute calibration needs to work properly, and the apparent cross section $d\Sigma_{\mathrm{app}}/d\Omega = i_1(d, q)/(\hat{I}Td)$ must be on scale. The original formula of Monkenbusch [2] tried to overcome this problem, but with our insight Eq. (10) becomes a little more complicated, i.e.:

$$\frac{\widetilde{d\Sigma}_{\mathrm{noncal}}}{d\Omega}(r) = \frac{\tilde{\imath}_1(d, 0)}{T_{\mathrm{ia}} - T} \cdot \ln\left(\frac{\tilde{\imath}_1(d, r)}{\tilde{\imath}_1(d, 0)}\frac{T_{\mathrm{ia}} - T}{T}\frac{1}{\tilde{R}_{\mathrm{P}}(r)} + 1\right) \tag{11}$$

The resulting non-calibrated scattering cross section Σ_{noncal} stays at the same level as the not necessarily calibrated intensity i_1. When taking the original prefactor from Eq. (10), namely $2\pi d^{-1}/\lambda^2$, instead of the actual one, $\tilde{\imath}_1(d, 0)/(T_{\mathrm{ia}} - T)$, the complete calibration is even done afterwards. The partial transmission $T_{\mathrm{ia}} = \exp(-\Sigma_{\mathrm{ia}}d)$ of incoherent and absorption needs to be known, when dealing with non-calibrated intensities. As one will see from the simulations below, the known neutron cross sections work well for this purpose, and one has the choice how to deal with this problem. The diligent experimentalist will possibly try all possible ways.

2. The analytical approach of incoherent scattering

The first successful attempt to solve the multiple scattering approach was presented by Chandrasekhar in his book [3]. In its own, the approach is exact and deals with arbitrary scattering functions also at wide angles. The problem lies in the numerical approach that already for incoherent scattering leaves with great uncertainties. I therefore tried an analytical approach to solve the integro differential equation of incoherent scattering and relied on Monte Carlo simulations as a thorough consistency check. For our purposes I obtained the result that in the small angle range the incoherent scattering is flat enough that it can be simply subtracted as the level where the intensity levels off. Therefore, no more detailed modeling is needed.

For the incoherent scattering intensity I redefine the functions according to $\hat{\jmath}_\pm(x, c) = j_\pm(x, c)/c$ and use the abbreviation $c = \cos\vartheta$. The original Eqs. (3) and (4) read now:

$$\pm c\partial_x\hat{\jmath}_\pm = \frac{\Sigma_{\mathrm{i}}}{4\pi}(I_0 + I_1) + \frac{\Sigma_{\mathrm{i}}}{2}\int_0^1 (\hat{\jmath}_+ + \hat{\jmath}_-)dc - \Sigma_{\mathrm{ia}}\hat{\jmath}_\pm \tag{12}$$

I can identify the inhomogeneity of the integro differential equations as $\frac{\Sigma_{\mathrm{i}}}{4\pi}(I_0 + I_1) = \frac{\Sigma_{\mathrm{i}}}{4\pi}\hat{I}\exp(-\Sigma_{\mathrm{ia}}x)$. One sees that the solutions $\hat{\jmath}_\pm$ depend linearly on this inhomogeneity, and so a generalized Green's function convoluted with the inhomogeneity might describe the solutions. Using an iterative method for solving this equation proves the convergence of the method and the existence of a solution. While it means solutions without the boundary condition of zero intensity for the incoherent scattering to each direction at its opposite face, I heuristically assumed a symmetry and tried to solve the equation with its inhomogeneity using mirrored images of the inhomogeneity (see Appendix). A quite simple semi-quantitative expression is obtained:

$$\hat{\jmath}_\pm(d \text{ or } 0) = \sum_{k=\pi(n+\frac{1}{2})d^{-1}} \frac{1}{1 \pm \frac{\mathrm{i}ck}{\Sigma_{\mathrm{ia}}}} \cdot \frac{A_1(k)}{1 - \alpha\frac{\Sigma_{\mathrm{ia}}}{k}\arctan\frac{k}{\Sigma_{\mathrm{ia}}} + \frac{1}{2}\alpha\frac{\Sigma_{\mathrm{ia}}}{k}\ln\left(1 + \frac{k^2}{\Sigma_{\mathrm{ia}}^2}\right)\sin(kd)} \tag{13}$$

The inhomogeneity $A_1 \sim I_0 + I_1$ is connected to the incoming intensity from other channels. All other factors in Eq. (13) together are a Green's function that is convoluted with the inhomogeneity in real space. So, this approach is considerably different from Chandrasekhar, but is limited so far to incoherent (isotropic) scattering. I feel that this approach is considerably easier than the quite mathematical approach by Chandrasekhar, which is supported by the shortness of the Appendix.

3. The ray tracing algorithm

As the second attempt, the most general approach for arbitrary sample geometries, wavelength spreads and other possible technical issues is obtained by ray tracing programs [7,8] that have the possibility to deal with many details. Each of the possible neutrons is represented by a single ray that is redirected inside the sample by the different scattering processes. The basic algorithm is already published in the web [9]. I tried a simplified algorithm that deals with inelastic incoherent scattering, meaning that a small fraction of incoherent scattering takes a single wavelength of approx. 1.2 Å [10,11], which results in a quicker escape of those neutrons from the sample. As long as the specific detector efficiency for those particular neutrons is not taken into account, the simulation of a reactor based instrument does not show real differences arising from the inelastic incoherent scattering. It surely has an effect for SANS instruments at spallation sources that, at the moment, I do not discuss. Also the details about neutron absorption could be neglected, because soft matter samples usually absorb weakly.

The neutron state in a ray tracing program [7] is represented by a position $\mathbf{x}$, a velocity $\mathbf{v}$ and an intensity information ω, which at a later point is modified by different weighting of probabilities. Apart from that, a time t accounts for the flight time from the source. Then, the wave-vector $\mathbf{k} = \mathbf{v} \cdot m_{\mathrm{n}}/\hbar$ can be obtained from the neutron mass m_{n} and the reduced Planck constant $\hbar = h/2\pi$. The neutron wavelength is given by $\lambda = 2\pi/|\mathbf{k}|$.

The ray tracing algorithm for the sample now calculates the path length Δx of a straight line in the sample along the velocity $\mathbf{v}$. The

probability for passing the sample without a scattering event is given by $p(\Delta x) = \exp(-\Sigma_t \Delta x)$, while the total probability for one single scattering event along the path is $p_{tot}(\Delta x) = 1 - p(\Delta x)$. I now introduce a lower boundary for the fraction p_{low} of flight paths that deal with scattered neutrons in order to describe the scattering to a high degree of statistical accuracy, while transmitted neutrons usually do not deserve such a high statistical accuracy. This correction is highly recommended for weakly scattering samples to keep the simulation times short. If however, the total probability is large, i.e. $p_{tot} > p_{low}$, then the random path inside the sample is given by $\Delta x_r = -\ln(r)/\Sigma_{tot}$ that is a simple inversion of the scattering probability $p(\Delta x)$ with a random variable r being equally distributed between 0 and 1. If the total probability is smaller, then the case of scattering and transmission need to be distinguished by a condition $r < p_{low}$ for scattering, again with a random variable r. In the case of scattering, the flight path is now $\Delta x_r = -\ln(1 - p_{tot} r)/\Sigma_{tot}$, and the weight of this particular simulation path needs to be modified via $w \leftarrow w \cdot \frac{p_{tot}}{p_{low}}$. Otherwise, the flight path Δx_r takes a tremendously large value for the time being, and the weight of the path is modified according to $w \leftarrow w \cdot \frac{1-p_{tot}}{1-p_{low}}$.

In the case of scattering, the particular scattering vector needs to be specified according to $Q = Q_{min} \exp(r \Delta q_{ln})$ with Q_{min} being a rather small minimum scattering vector that shall be considered, and the maximum scattering vector $Q_{max} = 2|\mathbf{k}|$. I define $\Delta q_{ln} = \ln(Q_{max}/Q_{min})$. The weight of the path is now modified as $w \leftarrow \pi w \Delta q_{ln} (Q/|\mathbf{k}|)^2 \cdot (d\Sigma_c/d\Omega(Q) + \Sigma_i/4\pi)/\Sigma_{tot}$. The scattering angle is $\vartheta = 2\arcsin(Q/2|\mathbf{k}|)$. The neutron is then redirected according to the azimuthal angle ϑ and an arbitrary polar angle ϕ at the scattering position according to Δx_r. For multiple scattering, the whole scattering problem is reiterated, now with Δx being the redirected residual flight path in the sample. For the higher order scattering processes, no scattering probabilities need to be redirected (i.e. p_{low} is set to 0 for the higher orders). The transmission case is indicated by $\Delta x_r > \Delta x$.

4. The computer simulations with experiments

There is already a study about multiple scattering of microemulsions in the literature [12]. The level of multiple scattering was kept at a reasonable level, and the emphasis was on the model parameters of the Teubner–Strey model [13]. I will argue that there are more aspects of multiple scattering, and I would argue on the level of incoherent background to be subtracted. As a strongly scattering sample I chose a microemulsion consisting of 41.5%$_{vol}$ heavy water, 41.5%$_{vol}$ n-decane, and 17%$_{vol}$ nonionic $C_{10}E_4$ surfactant. This microemulsion displays only little multiple scattering at a wavelength of 4.5 Å, while at 12 Å multiple scattering effects become severe (Σ_c changes from 1.55 cm^{-1} to 11.0 cm^{-1} respectively). The measurements and simulations of both wavelengths and two sample thicknesses of $d = 1$ mm and 2 mm are summarized in Fig. 2. All measurements are apparently calibrated by assuming single scattering processes only. The measurement at 4.5 Å and with 1 mm thickness was modeled using a modified Teubner–Strey model [14] with excess surface on the domain level. The formula reads:

$$\frac{d\Sigma_c}{d\Omega}(q) = \left(\frac{A_1}{q^4 - 2(k_0^2 - \xi^{-2})q^2 + (k_0^2 + \xi^{-2})^2} + \frac{A_2 \cdot \mathrm{erf}^{12}(1.06 q R_g/\sqrt{6})}{q^4 R_g^4} \right) \exp(-\sigma^2 q^2) \quad (14)$$

with the repeat distance of $d_{TS} = 216$ Å ($k_0 = 2\pi/d_{TS}$), a correlation length of $\xi = 115$ Å, two amplitudes of $A_1 = 1.86 \times 10^{-4}$ cm^{-1} sr^{-1} Å^{-4} and $A_2 = 984$ cm^{-1} sr^{-1}, the domain size of $R_g = 70$ Å, and a surfactant film roughness of $\sigma = 1.5$ Å. One sees an insufficiency of the model at the left side of the peak where the measured peaks appears sharper. This feature becomes more pronounced for stronger multiple scattering. For the time being, I neglected this detail because I did not have a better model function at hand.

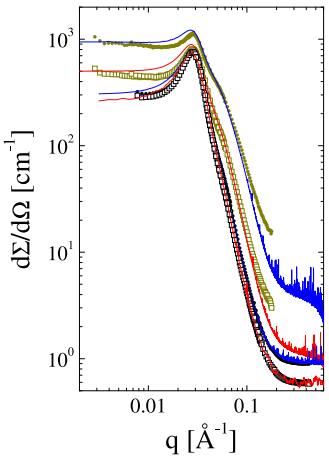

Fig. 2. The apparent cross section of several scattering experiments on the same microemulsion. Open black squares for 1 mm sample thickness and $\lambda = 4.5$ Å. Solid black dots for 2 mm, 4.5 Å. Open dark yellow squares for 1 mm, 12 Å. Solid dark yellow dots for 2 mm, 12 Å. The lines result from Monte Carlo ray tracing (red, blue, red, blue) with the scattering function obtained from the 1 mm, 4.5 Å experiment. (For interpretation of the references to color in this figure legend, the reader is referred to the web version of this article.)

For the incoherent scattering cross section, I could use the calculated one $d\Sigma_i/d\Omega = 0.256$ cm^{-1}sr^{-1} following the tables from the NIST web page [15]. This indicates, that multiple scattering occurs on the incoherent level already. For instance, it is known that normal water displays an incoherent scattering level of approx. 1 cm^{-1}sr^{-1} [16], while the calculated cross section is at 0.427 cm^{-1}sr^{-1}. The multiple scattering occurs when the first incoherent scattering process takes rather large angles near the lateral dimension of the sample. Then a second scattering process is probable. More neutrons are found in the forward direction (small angle range). This feature becomes more pronounced for the 4.5 Å and $d = 2$ mm measurement. The level is further off from the single scattering cross section. For the 12 Å measurements this tendency continues, but discrepancies between the simulations and the measurements start to appear. I speculate that other multiple scattering paths appear from the sample holder or other materials of the instrument that I neglected in the simulation. Apart from that, it is known that the coherent elastic and inelastic cross sections of water can vary dramatically with wavelength though [17].

The coherent multiple scattering becomes obvious with its overall raising level. Of course the coherent scattering features like the peak width [12] and the developing shoulder at approx. $q = 0.05$ Å^{-1} indicate the blurring properties of multiple scattering. The forward scattering grows with the higher scattering probabilities as well and is captured by the simulations. The growing shoulder is highly important for microemulsions, because the actual surface per volume is determined from the Porod constant, which determines the area of the surfactant head group [18]. In the model of Eq. (14) this shoulder could also be explained by the second term with its amplitude A_2, while in reality it is rather weak. Thus, the determination of the surface per volume has to be carefully analyzed in order not to obtain wrong values.

When coming back to the incoherent background level, I would like to argue that it can be taken as a level at higher (but not extremely high) q, where the intensity levels off. The examples of 12 Å wavelength could not access this rather high q-range, but from the simulations one sees that there is a plateau. In this sense the choice of wavelength can be seen as artificial, only to obtain large scattering cross sections, which might be true for stronger scattering samples even at 4.5 Å wavelength. Secondly, the real plateau value might even have contributions from the sample holder or other materials of the instrument that do clearly not originate from the sample alone. Thus, it is better to experimentally take

the plateau value before starting extensive simulations of the incoherent background.

5. The strategy for removing multiple scattering effects

From what I described above I would like to describe the strategy for removing multiple scattering effects, mainly from small angle neutron scattering experiments. In the near future, I would like to develop a software that is capable to perform these calculations. As already discussed, there are two prerequisites: (a) the wider angle scattering can be neglected, which is often true for soft matter samples, and (b) that the scattering events are clearly separated (which is usually also true for neutron scattering). Then I would describe the strategy in the following:

- The transmission must be measured in the beam center using a reasonably high resolution to separate the coherent and incoherent scattering from the primary beam.
- The apparent scattering cross section is calibrated by dividing by the term $\hat{I}Td$.
- Usually several detector distances are combined to cover a large q-range.
- The incoherent background can be taken from experiments as a level at reasonably high q, where the intensity levels off. In some rare cases it might appear as a plateau with a further decay at even higher q.
- For the apparent coherent cross section the incoherent background level is subtracted.
- The removal of multiple scattering (and possibly resolution effects) is done using Eq. (10) or (11). The diligent experimentalist might want to try both ways to see whether his calibration was correct, but needs to look up the cross sections for incoherent scattering and absorption.
- The needed Hankel transformation (i.e. 2-dim. Fourier transformation of isotropic signals) may be done best by creating interpolation points on a logarithmic scale. In this way, the different detector distances may be represented best.
- The second Hankel transformation is performed in the same manner.

If such calculations are performed on SANS data, it allows for a quick check, whether multiple scattering effects are present or not. If needed, the corrections can be used for further analysis. The corrections I discussed here do not involve a priori models, and, therefore, should not mislead the further interpretation.

For the microemulsion example one has seen that multiple scattering affects the appearance of the correlation peak and a shoulder. The shoulder usually is used to analyze the surface per volume and is connected to the surfactant head group area. In cases of strong multiple scattering this analysis will derive wrong values. Examples for such cases are large domain sizes and/or large wavelengths used to obtain the data.

In general, if the multiple scattering needs to be measured reliably – as for water as calibration standard – reproducible conditions need to be provided. The lateral propagation of neutrons is considerable, and so the neutrons leave the original window of exposure by 1 to 2 mm. So, the best condition would be a beam exit in the sample holder that leaves 1–2 mm more space in all directions. If this is not the case, the sample holder must consistently block those neutrons in all calibration measurements.

Appendix. The attempt of an analytical solution

Here I will give most of the details for solving the incoherent multiple scattering problem. The iterative method reads like this (with $\hat{J}_{\pm}(x,c) = \hat{J}_{\pm,1}(x) + \hat{J}_{\pm,2}(x,c) + \cdots$):

$$\left(1 \pm \frac{c}{\Sigma_{\mathrm{ia}}}\partial_x\right)\hat{J}_{\pm,1} = A_{\pm}(x) \tag{A.1}$$

$$\left(1 \pm \frac{c}{\Sigma_{\mathrm{ia}}}\partial_x\right)\hat{J}_{\pm,i} = \frac{\alpha}{2}\int_0^1 \left(\hat{J}_{+,i-1} + \hat{J}_{-,i-1}\right)dc \text{ for } i \geq 2$$

For the inhomogeneities $A_{\pm}$ images are allowed outside the interval $(0,d)$ to make sure for the boundary conditions. Since the boundary conditions are different for the forward and back direction, two different images are assumed. As one will see, the images are not simply constructed intuitively. The Fourier transformation with respect to x removes the differentiation, and so the operator can be moved to the right hand side. I arrive at:

$$\hat{J}_{\pm,1} = \frac{1}{1 \pm \frac{\mathrm{i}ck}{\Sigma_{\mathrm{ia}}}} A_{\pm}(k) \tag{A.2}$$

$$\hat{J}_{\pm,i} = \frac{1}{1 \pm \frac{\mathrm{i}ck}{\Sigma_{\mathrm{ia}}}} \frac{\alpha}{2} f^{i-2} \cdot \left(f \cdot (A_+ + A_-) + g \cdot (-A_+ + A_-)\right) \quad \text{for } i \geq 2 \tag{A.3}$$

$$f = \alpha \frac{\Sigma_{\mathrm{ia}}}{k} \arctan \frac{k}{\Sigma_{\mathrm{ia}}} \tag{A.4}$$

$$g = \frac{\mathrm{i}}{2}\alpha \frac{\Sigma_{\mathrm{ia}}}{k} \ln\left(1 + \frac{k^2}{\Sigma_{\mathrm{ia}}^2}\right) \tag{A.5}$$

The sum over all iterations finally results in:

$$\hat{J}_{\pm} = \frac{1}{2}\frac{1}{1 \pm \frac{\mathrm{i}ck}{\Sigma_{\mathrm{ia}}}} \left[\frac{1}{1-f}(A_+ + A_-) + \left(\mp 1 + \frac{g}{1-f}\right)(-A_+ + A_-)\right] \tag{A.6}$$

From the boundary conditions for all c I can derive two restrictions that read:

$$(A_+ + A_-) = -\left(g + \frac{\mathrm{i}}{2}(1-f)(\tan + \cot)\left(\tfrac{kd}{2}\right)\right)(-A_+ + A_-) \tag{A.7}$$

$$0 = (\tan - \cot)\left(\tfrac{kd}{2}\right)(-A_+ + A_-) \tag{A.8}$$

The latter equation motivates discrete k-values of $kd = \frac{\pi}{2} + \pi n$. This means that the whole system has to be considered periodic with $4d$ being the periodicity. For the allowed k-values I use the identity $(\tan + \cot)(\frac{kd}{2}) = 2\sin(kd)$, and I arrive at:

$$\hat{J}_{\pm} = \frac{1}{2}\frac{1}{1 \pm \frac{\mathrm{i}ck}{\Sigma_{\mathrm{ia}}}} \cdot \frac{1 \mp \mathrm{i}\sin(kd)}{(1-f) - \mathrm{i}g\sin(kd)}(A_+ + A_-) \tag{A.9}$$

While I identified the inhomogeneity, the residual terms in the equation above can be interpreted as a Green's function. In reciprocal space one sees a simple product while in real space it is a convolution. From here I still need to consider the boundary conditions in terms of symmetry for the term $(1 \mp \mathrm{i}\sin(kd))(A_+ + A_-)$. The symmetries of the individual factors of Eq. (A.9) finally lead to a final result, which reads:

$$(A_+ + A_-) = 2\frac{\alpha}{4\pi}\hat{I}\begin{cases} -\exp(-\Sigma_{\mathrm{ia}}(x+2d)) & \text{for } -2d < x < -d \\ +\exp(-\Sigma_{\mathrm{ia}}(x+d)) & \text{for } -d < x < 0 \\ +\exp(-\Sigma_{\mathrm{ia}}x) & \text{for } 0 < x < d \\ -\exp(-\Sigma_{\mathrm{ia}}(x-d)) & \text{for } d < x < 2d \end{cases} \tag{A.10}$$

The overall result can be simplified by combining the phases $(1 \mp \mathrm{i}\sin(kd))$ with the inhomogeneity. I define the new inhomogeneity A_1 now as follows:

$$A_1 = \frac{\alpha}{4\pi}\hat{I}\begin{cases} 0 & \text{for } -2d < x < -d \\ +\exp(-\Sigma_{\mathrm{ia}}(x+d)) & \text{for } -d < x < 0 \\ 0 & \text{for } 0 < x < d \\ -\exp(-\Sigma_{\mathrm{ia}}(x-d)) & \text{for } d < x < 2d \end{cases} \tag{A.11}$$

The discrete Fourier transformation is understood in the following by $A_1(k) = \frac{1}{4d}\int_{-2d}^{2d} A_1(x)\exp(-\mathrm{i}kx)dx$ and can be calculated analytically. The new overall result for the incoherent scattering functions reads now:

$$\hat{J}_{\pm}(x) = \sum_k \exp(\mathrm{i}kx) \cdot \frac{1}{1 \pm \frac{\mathrm{i}ck}{\Sigma_{\mathrm{ia}}}} \cdot \frac{A_1(k)}{(1-f) - \mathrm{i}g\sin(kd)} \tag{A.12}$$

Just the coordinates x have to be reinterpreted: For the transmission direction the x-values span the range $-d \ldots 0$, and for the backscattering direction x takes the classical values $0 \ldots d$. So, for the exiting intensities the x-value is simply zero in both cases, and the phase $\exp(\mathrm{i}kx)$ is unity. For the considered functions f, g, $\mathrm{i}\sin$, and A_1 the real parts are even, and the imaginary parts odd. For symmetry reasons, the observed intensities are real then, and the imaginary part can be neglected. The discrete sum is carried out numerically up to a finite $k_{\max}$-value, and the residual sum is replaced by an integral. The convergence is reasonable.

References

[1] J. Schelten, W. Schmatz, J. Appl. Cryst. 13 (1980) 385–390.
[2] M. Monkenbusch, J. Appl. Cryst. 24 (1991) 955–958.
[3] S. Chandrasekhar, Radiative Transfer, Dover Publications, New York, 1960.
[4] E.F. Semeraro, J. Möller, T. Narayanan, J. Appl. Cryst. 51 (2018) http://dx.doi.org/10.1107/S160057671800417X.
[5] C. Gerstl, M. Brodeck, G.J. Schneider, Y. Su, J. Allgaier, A. Arbe, J. Colmenero, D. Richter, Macromolecules 45 (2012) 7293–7303.
[6] J. Skov Pedersen, D. Posselt, K. Mortensen, J. Appl. Cryst. 23 (1990) 321–333.
[7] K. Lefmann, P.K. Willendrup, L. Udby, B. Lebech, K. Mortensen, J.O. Birk, K. Klenø, E. Knudsen, P. Christiansen, J. Saroun, J. Kulda, U. Filges, M. Konnecke, P. Tregenna-Piggott, J. Peters, K. Lieutenant, G. Zsigmond, P. Bentley, E. Farhi, J. Neutron Res. 16 (2008) 97–111.
[8] http://www.mcstas.org.
[9] http://www.mcstas.org/download/components/contrib/SANS_benchmark2.html.
[10] C. Do, W.T. Heller, C. Stanley, F.X. Gallmeier, M. Doucet, G.S. Smith, Nucl. Instrum. Methods Phys. Res. A 737 (2014) 42–46.
[11] R.E. Ghosh, A.R. Rennie, J. Appl. Cryst. 32 (1999) 1157–1163.
[12] J.A. Silas, E.W. Kaler, J. Colloid Interface Sci. 257 (2003) 291–298.
[13] M. Teubner, R. Strey, J. Chem. Phys. 87 (1987) 3195.
[14] C. Frank, H. Frielinghaus, J. Allgaier, H. Prast, Langmuir 23 (2007) 6526–6535.
[15] https://www.ncnr.nist.gov/resources/n-lengths/.
[16] P. Lindner, J. Appl. Cryst. 33 (2000) 807–811.
[17] J.R.D. Copley, Neutron News 18 (2007) 30–31.
[18] T. Sottmann, R. Strey, S.-H. Chen, J. Chem. Phys. 106 (1997) 6483–6491.